Noise Reduction Potential of Phase Control for Distributed Propulsion Vehicles

Kyle A. Pascioni*, Stephen A. Rizzi†, and Noah H. Schiller‡
NASA Langley Research Center, Hampton, VA 23681

Phase control is a noise reduction technique leveraging destructive interference of the coherent acoustic source field between a system of propellers rotating at equivalent rates. Carefully selecting the relative azimuthal blade positions (phase), the overall directivity of the blade passage frequency noise can be modified, potentially steering these tonal components away from sensitive areas. A modeling technique is described and validated using measurements of a dual-rotor system. The sensitivity of noise reduction through phase control is studied in a typical parameter space, i.e., dependence on rotation rate, number of propellers, spacing and layout, and rotation direction. Additionally, estimates of how realistic conditions, e.g., error in the phase controller, degrade potential benefits are described based on the generalized coherence of the system. From this, it is observed that the deviation from the nominal rotation rate should not exceed approximately 0.5% to achieve a 6 dB decrease at the blade passage frequency.

Nomenclature

A	Pressure amplitude, [Pa]
$\tilde{A}$	Interpolated pressure amplitude on source hemisphere, [Pa]
c_0	Sound speed, [m/s]
d	Hub-to-hub distance between two rotors, [m]
D	Propeller diameter, [m]
$f,\ f_0$	Frequency vector and blade passage frequency, [Hz]
k	$= 2\pi f/c_0$, Acoustic wavenumber, [rad/m]
m	Observer index
M	Number of observers
n	Propeller index
n_h	Harmonic index
N_b	Number of blades per propeller
N_H	Number of harmonics
N_p	Number of propellers
$p(t)$	Acoustic pressure time history, [Pa]
SPL	Sound pressure level, [dB re. 20 μPa]
$r_{m,n}$	Distance between observer m and propeller n, [m]
R	Propeller radius, [m]
R_s	Radius of source hemisphere, [m]
t	Time vector, [s]
$\mathbf{x}$	$= (x_1, x_2, x_3)$, Observer coordinates, [m]
$\mathbf{X}$	Matrix of cross power terms
$\mathcal{Z}_i$	ith region of ground noise contour
β	Modulation index
Δ	Difference in SPL between phase controlled case and reference at a single point in space, [dB]

*Research Aerospace Engineer, Aeroacoustics Branch, Member AIAA
†Senior Researcher for Aeroacoustics, Aeroacoustics Branch, Fellow AIAA
‡Research Engineer, Structural Acoustics Branch, Member AIAA

$\Delta_{\mathcal{Z}_i}$	Spatially averaged difference in SPL between phase controlled case and reference over region $\mathcal{Z}_i$, [dB]
γ	Complex coherence function
$\bar{\gamma}$	Generalized coherence function
$\hat{\lambda}$	Eigenvalue of complex coherence spectral matrix
Ω	Propeller rotation rate, [rad/s]
σ	Standard deviation of Gaussian phase noise, [rad]
$\mathbf{\Sigma}$	Complex coherence spectral matrix
$\psi,\ \psi_r$	Propeller azimuthal angle and relative phase angle, indexed over the full propeller azimuth, ψ_{total}, [rad]
ψ_{total}	$= 2\pi$ over the full propeller azimuth, [rad]
$\tilde{\psi}$	Interpolated phase on source hemisphere, [rad]
ϕ	Elevation angle, [deg.]
φ_e	Random phase to decorrelate motor control error, [rad]
τ	Propagation time, [s]

I. Introduction

DISTRIBUTED electric propulsion (DEP) systems are becoming increasingly popular because of their ability to distribute propulsors in many locations on the vehicle, not just near the power source. For aircraft designers, DEP opens up new degrees of freedom within aerodynamics, vehicle control, and acoustics, to name a few. New unmanned aerial vehicles (UAVs), urban air mobility (UAM) systems, and thin/short haul aircraft concepts exploit DEP for different purposes. Noise is anticipated to be one of the key barriers to entry into service for these platforms.

Many vehicle concepts[1–3] in these classes are expected to have a forward flight mode for cruise, employing a multipropeller system (propellers being axially or near-axially aligned with the flight direction), and a vertical takeoff and landing (VTOL) capability. In certain configurations, transition from VTOL to forward flight is achieved via a wing and tail tilt command to convert a multirotor system to a multipropeller system.

Recently, a number of studies have made progress with source noise identification of small scale vehicles for aerodynamic propulsion noise,[4–6] electric motor noise,[7] and effects of rotor/airframe interaction.[8] But, there is a current lack of knowledge as to what noise sources dominate for a given vehicle configuration at a specified set of operating conditions. Unsteady loading due to installation effects (nearby surfaces altering the otherwise uniform mean streamlines) and/or interaction effects (blade-wake or rotor-rotor interaction) can yield a significant increase in harmonic content under certain circumstances. Nonetheless, steady tonal aerodynamic noise is expected to dominate some subset of the vehicle operating range, particularly when a vehicle is acoustically optimized. The work herein will make this assumption and attempt to determine the benefit of introducing a noise reduction technology, namely phase control, to a distributed propulsion system.

Phase control is defined as controlling the relative angular blade positions of a set of propellers (or potentially rotors) rotating at equivalent rates. In doing so, destructive interference of the coherent acoustic source field can be leveraged to ultimately modify the overall vehicle directivity. Without phase control, satisfying a noise constraint in sensitive areas (communities, schools, etc.) would likely necessitate a change in the flight path or in the operational state – the byproduct often being a detriment to performance. By steering noise (more specifically, the steady tonal aerodynamic noise generated by rotating blades) away from these sensitive areas via phase control, the change in flight path/operation state is anticipated to be less severe. Thus, the performance to acoustic tradeoff can be improved.

Building upon previous work,[9,10] the potential noise reduction benefit of phase control is assessed. Similar to synchrophasing of conventional propeller driven aircraft in an effort to minimize cabin noise,[11,12] the phase of each noise source at the blade passage frequency is specified to cancel the noise radiating in certain directions. Under ideal conditions, the average sound exposure level of a representative vehicle with a distributed propulsion system, the GL-10,[1] could be reduced by 6.4 dB in forward flight for a single flyover event.[10] Degradation of this ideal benefit is inescapable as realistic effects are encountered. For instance, error in the motor controller attempting to enforce a prescribed phase angle can decorrelate the radiating acoustics if the rotation rate is slightly changed, or if the relative phase is not held constant between two or more propellers. To this end, various vehicle parameters, e.g., propeller layout, the number of propellers, rotation

rate, and rotation direction will be examined to understand their influence on phase control performance. Another objective here is to understand, to what degree, realistic environments degrade potential benefits.

This paper is structured as follows. First, the noise prediction method is presented, followed by validation of the methods using acoustic measurements of a dual-rotor system under static conditions. Then, canonical vehicle configurations, the chosen operating conditions, and the reference cases are defined. The procedure for estimating the benefit of phase control is then discussed, including the optimization method to determine the best phasing combination for an acoustic-based objective at given vehicle states. Noise reduction benefits under ideal conditions are then quantified to understand their sensitivity to the parameter space. Impositions of two types of motor control error are also estimated.

II. Methodology

II.A. Noise Prediction Method

Following the method of Pascioni and Rizzi,[9] the Propeller Analysis System[13] (PAS) module of the Aircraft NOise Prediction Program[14] (ANOPP) is used to estimate the tonal acoustic signature of multi-propeller/multirotor systems. The reader is referred to Pascioni and Rizzi[9] for a detailed schematic and discussion using similar nomenclature. In summary, the steady blade surface pressures are estimated via blade element momentum theory. With the blade geometry and blade loading defined, two types of deterministic tonal noise, thickness and loading noise, are predicted using Farassat's F1A formulation[15] of the FW-H equation. The magnitude and phase of the Fourier-transformed pressure-time histories, individually per propeller, are each stored on "source hemispheres" with a radius of $R_s = 12R$, R being the propeller radius, at a 5 degree resolution. The harmonic sequence is truncated above the fifth blade passage frequency due to the rapid roll-off in amplitudes. The source hemispheres are distributed in space according to the propeller layout of the canonical vehicles discussed in section II.C. A ground plane with a set of observer locations $\mathbf{x} = (x_1, x_2, x_3)$ is centered on the vehicle center of gravity (CG) and moves with the aircraft. Hence, there is no Doppler shift embedded in these simulations. Atmospheric absorption is not modeled, as it is assumed to have a small effect at the frequencies and length scales investigated here. Straight rays from each propeller to each ground observer determine the propagation paths. The intersection of these rays with the source hemispheres determines the query points where the complex acoustic pressures are interpolated. The process is repeated for each propeller in the configuration under study. The influence of the airframe (nearby reflecting/scattering surfaces) is not accounted for at this time.

The interpolated (frequency-domain) pressure is then adjusted to account for propagation time and spherical spreading. To clarify, let the acoustic pressure of a given frequency at the interpolation point on the source hemisphere have pressure amplitude $\tilde{A}$ with phase $\tilde{\psi}$. We will use the notation $\tilde{(\cdot)}$ to denote an interpolated value. Knowing the distance between propeller n and the observer m, $r_{m,n}$, spherical spreading loss is accounted for by scaling the amplitude based on the additional distance, i.e., $p_m/\tilde{A}_m \propto R_s/r_m$. The propagation time can also be found as $\tau = (r_{m,n} - R_s)/c_0$. Finally, the contributions of each propeller can be linearly summed at observer m to generate a time series,

$$p_m(t) = \sum_{n=1}^{N_p} \sum_{n_h=1}^{N_H} \frac{R_s}{r_{m,n}} \tilde{A}_{m,n_h,n} \sin(\Psi). \tag{1}$$

Noting that the acoustic frequencies of the harmonic sequence are related to the propeller rotation rate by the number of blades, N_b, and $f_0 = N_b\Omega/(2\pi)$,

$$\Psi = N_b n_h \Omega(t - \tau) + \tilde{\psi}_{m,n_h,n} + N_b n_h \psi_{r_n} \tag{2}$$

in which n_h is the harmonic index. The summation occurs across the number of harmonics, N_H, and the number of propellers, N_p. Note that PAS can model a propeller rotating in both a counterclockwise or clockwise fashion. Thus, no sign change is needed in equation 1 or 2 to incorporate different rotation directions, as they are already captured in the $\tilde{(\cdot)}$ quantities. The last term of equation 2, $\psi_{r,n}$, adjusts the relative angular blade position (or phasing) on the interval $[0, 2\pi)$ of the full azimuth. The phase of one propeller is typically taken as a reference, such that $\psi_{r,1} = 0$. N_b is used to index the phase based on azimuthal periodicity and n_h is used to retain the relative phase of the harmonic sequence so as to not distort the waveform. Time dependence of the final form is preferred over a frequency-domain formulation to permit any noise metric of interest to be calculated.

II.B. Experimental Validation

As mentioned, a requirement for altering the acoustic directivity of the propeller tones for a given vehicle via phase control is that the propellers must be rotating at equivalent rates. To ensure the methods of the previous section are capturing the resulting acoustic radiation patterns of the combined coherent source fields, a dual-rotor experiment is used for validation.

Figure 1 provides an image of the rotor hardware and measurement setup. Each rotor has a set of two blades manufactured by KDE Direct, model CF125,[†] with a radius $R = 0.159$ m and the hub separation distance $d = 0.4$ m. Relative phase is mechanically set and held constant for a given run. Timing belts drive both shafts simultaneously; hence, not only is the relative phase constant, so too is the relative rotation rate. Note that this drivetrain setup is used here for convenience, but electronically controlled phasing is expected to be used in practice. The testbed is installed in the anechoic chamber of the Structural Acoustics Loads and Transmission (SALT) facility,[16] which has a low frequency cutoff of 100 Hz. The rotation rate is set to 5,100 RPM, resulting in a fundamental blade passage frequency f_0 =170 Hz. Microphones are located in a circular elevation arc 1.9 m (approximately a wavelength at f_0; roughly $10R$) from the center of the rotor system. For brevity, however, only the in-plane microphone ($\phi = 0°$) will be used herein. To acquire data at different azimuthal angles but with the same microphone, the rotor system rotates as a whole about its mounting rail.

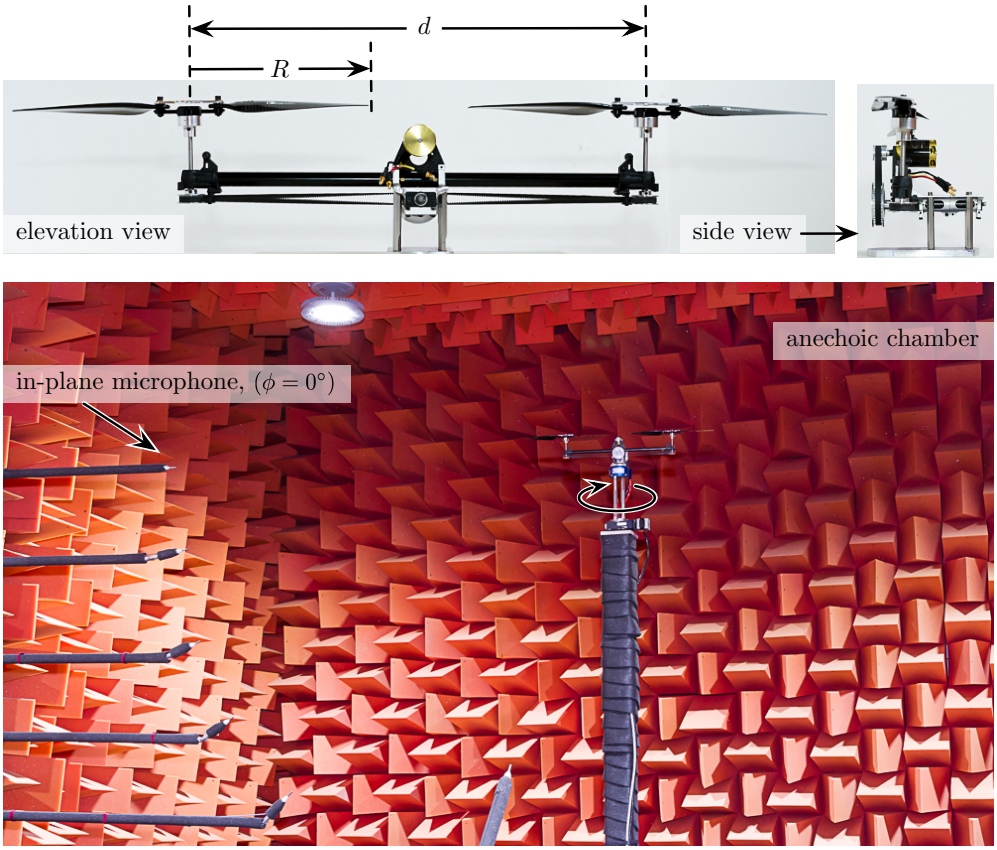

Figure 1. Dual phase-locked rotor testbed (*top*), where $R = 0.159$ m and $d = 0.4$ m, and the testbed is installed in the Structural Acoustics Loads and Transmission facility. Only the data acquired at $\phi = 0°$ elevation relative to the rotor blades will be used herein.

It is known that large differences are typically associated with static rotor acoustics in an enclosed environmental versus forward flight propeller acoustics. In addition to the difference in mean inflow velocities, flow recirculation in the room can drastically change the harmonic content of the rotor noise. The rotor wake quickly (on the order of seconds) wraps around the chamber and is pulled through the rotor resulting

[†]This blade set is only used here for the validation stage. A similar but different blade geometry is used in section III.

in random unsteady loading events. The byproduct is a large increase in loading noise. In some cases, the differences can exceed 20 dB relative to a rotor interacting with clean, uniform flow. The fundamental blade passage frequency, however, which is tied to steady loading, is found to have a very small variation in both levels and directivity patterns. Thus, the data are extracted at f_0 in the results that follow. Additional details on the experimental setup can be found in Schiller et al.[17]

Figure 2 provides the comparison of the in-plane azimuthal levels at the blade passage frequency between the current methods outlined in section II.A and the experimental data. Several conditions are compared. First, Fig. 2(a) suggests the numerical model has the ability to predict the noise of an isolated rotor quite well. While PAS is fundamentally a propeller noise code, good agreement is found by introducing a change in the coordinate system and reducing the inflow velocity to 1 m/s (in an attempt to approach the limiting condition of a hovering rotor). This finding has been corroborated by others.[4,9]

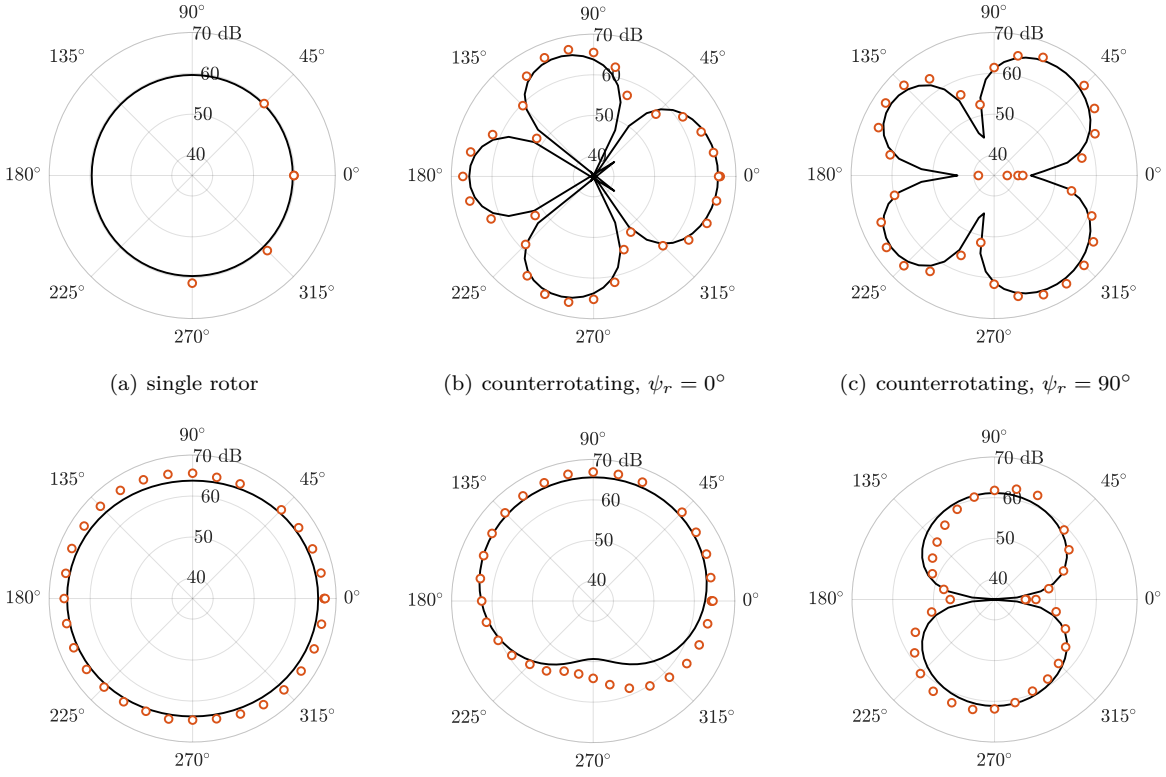

(a) single rotor (b) counterrotating, $\psi_r = 0°$ (c) counterrotating, $\psi_r = 90°$

(d) corotating, $\psi_r = 0°$ (e) corotating, $\psi_r = 45°$ (f) corotating, $\psi_r = 90°$

Figure 2. Comparison of azimuthal blade passage frequency levels at $\phi = 0°$ elevation of the current prediction method (solid lines) and a two-bladed dual-rotor static test ('○') for various relative phase, ψ_r, and relative rotation directions; all rotating at a rate of 5,100 RPM.

Figures 2(b) and 2(c) give the predicted and measured levels for cases when the rotor rotation directions oppose each other. A relative phase offset of $\psi_r = 0°$ results in a four leaf clover pattern. This lobe pattern likely occurs because the distance between the bladeset of one rotor is modulated relative to the other bladeset. When $\psi_r = 90°$, the clover pattern rotates about the azimuth as the relative blade positions change in absolute space. This rotation is also consistent with a change in phase between a pair of monopoles.[18]

The rotor directions were also set to the same direction, i.e., corotating, as shown in Figs. 2(d) to 2(f). When $\psi_r = 0°$, the rotors are in phase, and due to the fact that the rotors act like an acoustically compact system (i.e., $kd = 1.25$ where k is the acoustic wavenumber), the propagating acoustics are also at a near in-phase condition at all emission angles. Hence, levels are 4-5 dB higher than that of the isolated rotor case, approaching the theoretical 6 dB increase of two colocated in-phase monopoles. Azimuthal asymmetry is found in Figs. 2(e) and 2(f) when $\psi_r \neq 0°$. When $\psi_r = 90°$, the resulting acoustic waves are actually 180° out of phase. Recall that the acoustic phasing is dependent on the number of blades (refer to the last term of eqn. 2 and noting $n_h = 1$ here). That is, the acoustic phasing is $N_b\psi_r$. This is the reason why a clear dipole pattern is observed. Qualitatively comparing the lobe structures observed here versus the counterrotating

pair, the corotating case looks to be better suited for minimizing noise over a larger range of emission angles. These differences will be discussed in more detail in section III.

All in all, good agreement is found for an isolated rotor and the dual-rotor system with both relative rotation directions. The largest deviation between analysis and experiment occurs when $\psi_r = 45°$ for the corotating case. While the reasons for this are not known, this could be due to slight misalignment when manually setting the relative phase for this case.

II.C. Canonical Vehicle Configurations and Conditions

Several propeller layouts are studied to understand the differences in potential noise reduction capability. Figure 3a shows two main configuration types, a 1D and 2D array, varying the number of propellers from 2 to 8. The 1D array may represent a distributed propulsion system along the wing, while the 2D array is chosen due to the expectation of more uniform reduction at all emission angles. For all configurations, the propeller spacing is one diameter ($d = D$) in both directions.

The propeller geometry chosen is the three-bladed APC 16x8 ($D = 0.4064$ m), that used on the GL-10 vehicle.[1] Keeping the dimensional separation distance constant, the rotation rate will be changed to study the effect of acoustic compactness, which will be quantified using kd. Surveying the operational envelope of these propellers, a low, medium, and high rotation rate correspond to 3,500, 5,000, and 8,000 RPM, respectively. The flight speeds are set to 14, 20, and 32 m/s, respectively, to keep the advance ratio constant at approximately 0.6. The following analysis is under the assumption the flight conditions remain constant. No maneuvers or transient effects are included.

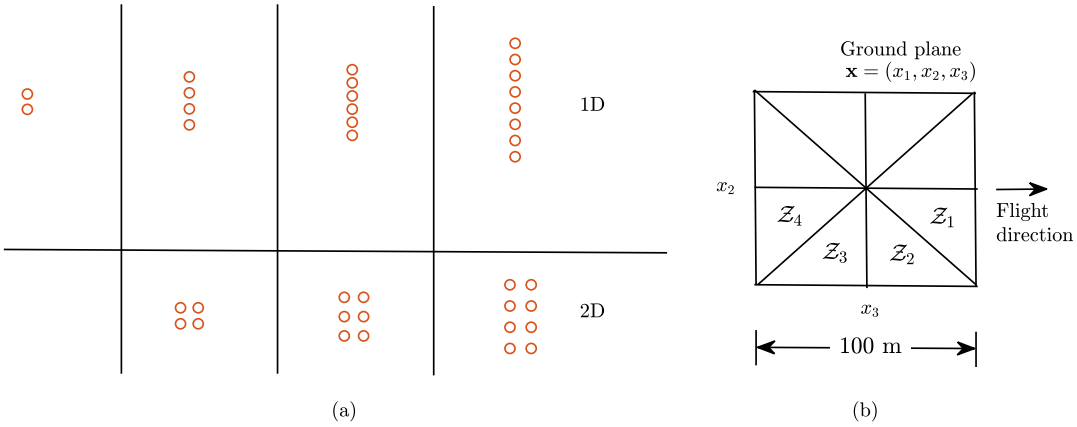

Figure 3. Top view of the (a) canonical propeller layouts and (b) square ground plane broken into 45° emission wedge angles. The '○' denotes the position of each propeller hub, with spacing of one propeller diameter in both directions.

II.D. Determination of Relative Phasing

The expected number of propellers and many DEP configurations make it intractable to use equation 1 to study all possible phase combinations to find an optimum. In general, the number of combinations is $N_c = (2\pi/(\Delta\psi_r N_b))^{N_p-1}$, where $\Delta\psi_r$ is the azimuthal resolution in radians defined relative to the total azimuth. The exponent is one less than N_p as one propeller is treated as the reference, e.g., $\psi_{r,1} = 0$. For example, if $N_p = 10$ and the azimuth is discretized in an increment $\Delta\psi_r = 0.0175$ rad. (1°), $N_c = \mathcal{O}(10^{18})$. Making matters worse, this calculation should be performed for every flight condition and noise reduction region of interest. To limit computational expense and following work of the antenna community (see, for example, Ares-Pena et al.[19] and Boeringer & Werner[20]), optimization techniques are employed to solve for the phase angles.

The optimization problem is given by the following expression,

$$\min \left\{ \frac{1}{M} \sum_{m=1}^{M} p_{rms,m}^2(f_0) \right\}, \quad \text{s.t. constraints.} \tag{3}$$

That is, the average mean square pressure of the blade passage frequency over a subset of observers is sought to be minimized. The acoustic performance assessment will include the first five harmonics. The observer subsets are equal-area distributed points on the ground plane inside region $\mathcal{Z}_i$, such that $M \in \mathcal{Z}_i$. For instance, a single optimization run will use the ith 45° emission wedge angles as depicted in Fig. 3b. The vertical distance from the ground plane to the CG coincides with a cruise altitude of 30.5 m. In this work, the propeller phase sets are optimized independently for each wedge. Only the starboard side of the ground plane is considered because the conditions studied enforce symmetry about the vehicle's roll axis. In other words, any noise reduction that can be obtained on the starboard side can be matched on the port side. Also, no constraints are imposed on other observers here, but these could be introduced later during optimization. For example, it may be desired to spread acoustic energy more evenly among emission angles thereby reducing the maximum SPL at any given observer.

The interior point algorithm[21] via the `multistart` implementation of `fmincon`[22] is used for the optimization. Essentially, the optimization is run per case for 200 different initial value sets to avoid getting stuck in local minima. A Sobol sequence[23] is defined to randomly distribute the initial values efficiently over the phase space. The phase set that minimizes the objective function across the multiple runs is chosen. Reasonable trends across different cases gave confidence that a global minimum (or at least a local minimum close to the value of the global minimum) was captured.

II.E. Reference Case

To quantify the noise benefit associated with phase control, a reference case must be established. Because these vehicles are expected to have propellers driven initially by independently operating motors (without phase control), a fixed relative phase is not the most appropriate baseline. Instead, the average levels over 1,000 random phase combinations serve as the reference. Figure 4 gives examples of the ground noise contours of this statistical average for the 1D four propeller configuration. Normalized by their maximum sound pressure level, the contours look very similar among three different rotation rates, although the highest rotation rate looks to have slight bias in the aft direction due to increased loading noise.

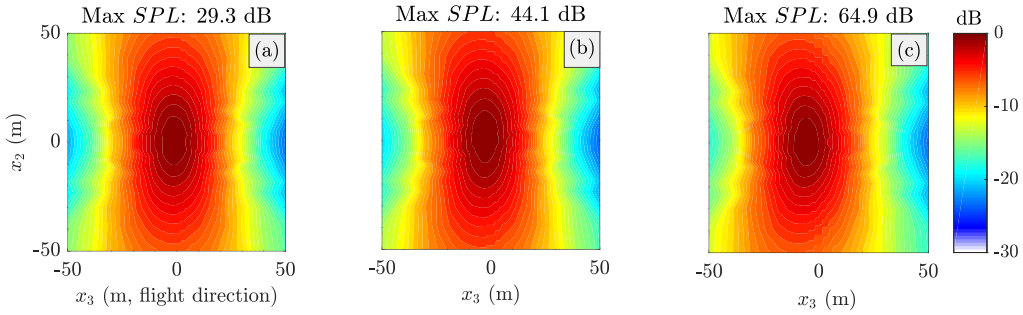

Figure 4. Example of the stochastic average result serving as the reference levels. The 1D, $N_p = 4$ configuration is given for (a) 3,500, (b) 5,000, and (c) 8,000 RPM. Levels are normalized by the maximum, per plot.

II.F. Simulating Realistic Effects

Similar to active noise control systems and limiting the discussion to a single point in space, the fundamental limits of performance (in dB) can be established between two signals, x_i and x_j, of equivalent amplitudes and 180 degrees out of phase. This limit at a given frequency is based on their coherence,[24]

$$\Delta = 10 \log_{10} \left[1 - |\gamma_{x_i x_j}(f)| \right], \tag{4}$$

relative to the power of their incoherent sum, in which $\gamma(f) = S_{x_i x_j}(f) / \sqrt{S_{x_i x_i}(f) S_{x_j x_j}(f)}$ is the complex coherence function with dependence on the auto- and cross-spectral density functions, $S_{x_i x_i}$ and $S_{x_i x_j}$, respectively. Figure 5(a) plots this equation for reference. As $|\gamma| \rightarrow 1$, two out of phase signals have the capacity to completely cancel one another at the frequency of interest (represented by $\Delta \rightarrow -\infty$ from equation 4). Applied to acoustics, this relationship holds for a point in space but may introduce amplification at other locations. When $|\gamma| = 0$, the two signals are completely decorrelated and thus cannot cancel one

another ($\Delta = 0$ dB). In this paper, the ideal case assumes a coherence of unity. In reality, however, errors deriving from practical considerations (e.g., error of the motor controller) reduce the coherence such that $0 \leq |\gamma| < 1$ between the radiating acoustics of any given set of propellers.

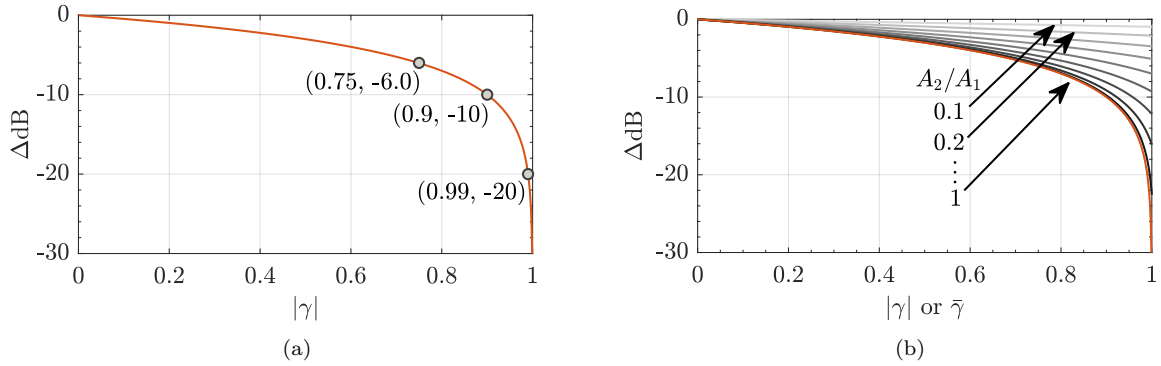

Figure 5. Noise reduction potential at a single point in space as a function of coherence of two signals for (a) equivalent amplitudes and (b) nonequal amplitudes.

For this work, it is more convenient to generalize equation 4 for systems with more than two signals (propellers). This would allow a single valued metric to estimate the system potential. Following the work of Ramirez, Via, and Santamaria,[25] and defining a matrix $\mathbf{\Sigma}(f) \in \mathbb{C}^{N_p \times N_p}$ containing the complex coherence spectra of each signal pair,

$$\mathbf{\Sigma}(f) = \begin{bmatrix} 1 & \gamma_{x_1 x_2}(f) & \dots & \gamma_{x_1 x_{N_p}}(f) \\ \gamma_{x_2 x_1}(f) & 1 & \dots & \gamma_{x_2 x_{N_p}}(f) \\ \vdots & \vdots & \ddots & \vdots \\ \gamma_{x_{N_p} x_1}(f) & \gamma_{x_{N_p} x_2}(f) & \dots & 1 \end{bmatrix}, \tag{5}$$

an estimate of the generalized magnitude coherence can be formulated as

$$\bar{\gamma}(f) = \frac{1}{N_p - 1}(\max\{\hat{\lambda}(\mathbf{\Sigma}(f))\} - 1). \tag{6}$$

That is, the generalized coherence of the system is estimated using the dominant eigenvalue, $\hat{\lambda}_{\max}$, of the complex coherence spectral matrix. Using this new definition, the limit of acoustic performance can be estimated by equation 4 remembering the restriction of equivalent amplitudes and assuming the phases are set appropriately, i.e., $\psi_{r,n} = 2\pi(n-1)/N_p$. Although not the case for the current work, if N_p signals have different pressure amplitudes, the generalized coherence alone does not capture the limit of acoustic performance. Defining a matrix $\mathbf{X}$ to gather the interference power terms,

$$\mathbf{X} = \begin{bmatrix} 0 & A_1 A_2 \cos(\psi_{r,1} - \psi_{r,2}) & \dots & A_1 A_{N_p} \cos(\psi_{r,1} - \psi_{r,N_p}) \\ 0 & 0 & \ddots & \vdots \\ 0 & 0 & 0 & A_{N_p - 1} A_{N_p} \cos(\psi_{r,N_p - 1} - \psi_{r,N_p}) \\ 0 & 0 & 0 & 0 \end{bmatrix}, \tag{7}$$

the limit of performance in this situation can be given as

$$\Delta = 10 \log_{10} \left[1 + \frac{2\bar{\gamma} \hat{\mathbf{e}}^T \mathbf{X} \hat{\mathbf{e}}}{\sum_{i=1}^{N_p} A_i^2} \right], \tag{8}$$

in which $\hat{\mathbf{e}}$ is an $N_p \times 1$ unit vector. Figure 5(b) plots this equation for two signals with different amplitudes. Such a situation would arise if the propellers are at an angle of attack as the directivity diverges from azimuthal symmetry, or if there are differences in blade pitch among the propeller system.

While much can be learned through interpretation of the relations above, recall they are only valid for a single point in space. Extensions can be formulated to include spatial effects.[24] This is essentially what section III will do numerically to allow inclusion of source directivity for the individual propellers.

II.F.1. Motor Control Error

Two types of control error will be discussed: a time-varying error in the relative phase setpoint and an error in the rotation rate. Both reduce the coherence in the source field. To model the first situation, a statistical approach is taken by adding random noise to each phase setpoint. Pulling from a Gaussian distribution in which the standard deviation σ will be used to define the magnitude of the phase error, a time series is generated by stitching individual blade passage events together with the phase error. In other words, the phase argument in equation 2 for the ith blade passage event becomes

$$\Psi = N_b n_h \Omega(t-\tau) + \tilde{\psi}_{m,n_h,n} + N_b n_h \psi_{r_n} + \left(\frac{1}{2\pi\sigma} e^{-\frac{(z - N_b n_h \psi_{r_n})^2}{2\sigma^2}} \right)_{z=z_i}, \tag{9}$$

in which z_i is a sample of the distribution. Figure 6 gives an example of how the coherence and potential benefit between a pair of signals degrade with an increase in the standard deviation of the added noise. The analysis is performed for a two-propeller system with different numbers of blades to show how the relative error amplifies with increasing blade count.

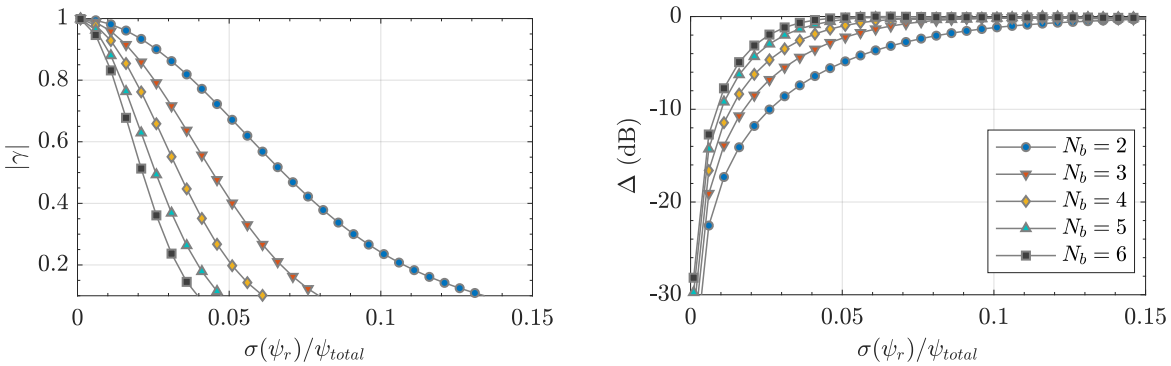

Figure 6. (a) Coherence degradation as a function of the standard deviation of the added noise to the relative phase setpoint. (b) Noise reduction potential as a function of standard deviation of the added noise.

For propellers with electronic phase control, the rotation rates will not always be perfectly matched. Rather, the controller will have to continuously compensate for electronic drift or environment interaction such as wind gusts. Similar to previous studies which employed a frequency modulation,[9,26] the new phase argument is given as follows,

$$\Psi = N_b n_h \Omega(t-\tau) + \tilde{\psi}_{m,n_h,n} + N_b n_h \left(\psi_{r_n} + \beta \cos(\Omega_{mod} t + \varphi_{e,n}) \right), \tag{10}$$

in which $\beta = \Delta\Omega/\Omega_{mod}$ is the modulation index. The modulation frequency, Ω_{mod}, is set to 31.4 rad/s (5 Hz) to demonstrate the effect. This modeling method can extract the reduction of phase control potential in a time-averaged sense. In other words, we are not attempting to capture the dynamics associated with the controller. The term $\varphi_{e,n}$ is needed to model independent control of each propeller. That is, the phase errors among propellers are not synchronized. Excluding $\varphi_{e,n}$ would lock the phase error of all propellers and virtually increase the coherence between the acoustic signals across the propeller array. Similar to the phase setpoint error, a Monte Carlo simulation is performed varying $\varphi_{e,n}$ for a given control error.

Figure 7 provides the same trends as Fig. 6 for the error described in equation 10. Again, the relative error is increased with a higher blade count due to azimuthal periodicity. Experience with motor controllers suggest a 20-30 RPM deviation should be expected using current technology. Under these circumstances, the coherence is approximately 0.8 for a three-bladed system, resulting in approximately an 8 dB benefit. In section III.B, the same error will be applied, but the potential benefits will be averaged over a region of the ground plane rather than at a single point.

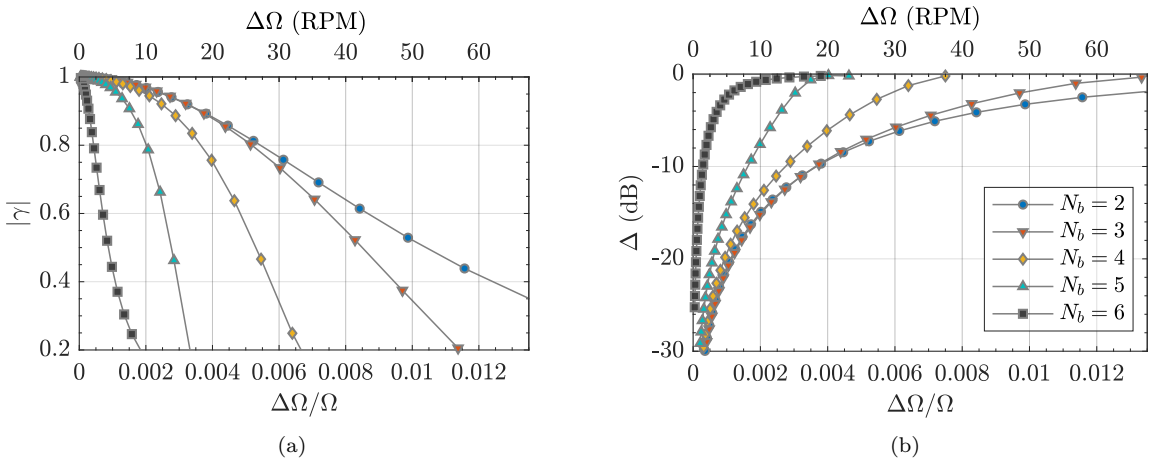

Figure 7. Coherence degradation as a function of the modulation frequency deviation to model RPM error. (b) Noise reduction potential as a function of frequency deviation for different numbers of blades.

II.F.2. Comments on Other Propulsive Noise Sources

Alongside steady periodic thickness and loading noise, three other categories of propulsive noise may be important contributors, ultimately setting an effective noise benefit floor. Restricting this discussion to constant nominal flight conditions (no maneuvers), unsteady periodic noise can be caused by a spatially dependent but a non-time varying inflow condition. Note that this category includes a non-axially aligned uniform freestream, e.g., a non-zero angle of attack, but also includes potential field effects caused by nearby surfaces. For instance, a fuselage or a downstream wing could cause spatial velocity gradients in the plane of a nearby propeller. For best results, the vehicle configuration or set of operating conditions chosen to apply phase control should be void of these effects as much as possible. Unsteady aperiodic loading noise can be generated by random events such as wind gusts, atmospheric turbulence, or wake ingestion of another element. Even though wind gusts and atmospheric turbulence are inescapable, if they occur in a short period of time relative to the duration of a flyover event, phase control may still be useful as the integrated noise signature (sound exposure level or other certification metrics of the like) may still be significantly reduced.

Additionally, electric motor noise is typically tonal and can be appreciable in the kHz range. For example, Fig. 8 is a representative measured acoustic spectrum of an isolated Mejzlik propeller (zero degree angle of attack) installed in the Low Speed Aeroacoustic Wind Tunnel (LSAWT)[27] at NASA Langley Research Center. This propeller geometry is different than that used in section III, but has similar characteristics. While the level at f_0 dominates, motor noise is clearly also an important contributor, and potentially the most significant in an A-weighted sense. Broadband noise, however, is expected to be low for propellers and is of secondary importance here (but that may not be the case for rotors in edgewise flight).

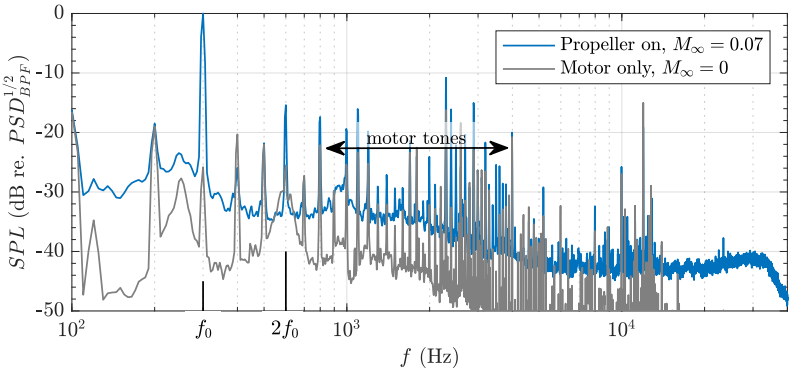

Figure 8. Representative spectra of an in-plane acoustic measurement of a three-bladed Mezjlik propeller in the LSAWT.

Given these remarks, caution should be employed when estimating the benefits of phase control without understanding the relative importance of other noise sources and modification of those sources due to propagation. The following section will not impose an effective noise floor. Instead, the attempt here is to understand under what conditions phase control will be the most successful.

III. Potential Noise Benefits of Phase Control

The following section begins by discussing trends observed over various propeller layouts, number of propellers, rotation rates, and relative rotation directions where a coherence of unity is assumed. Then, this assumption will be relaxed to understand the sensitivity to motor control error defined in the previous section.

III.A. Ideal Conditions

To get an idea of the ideal response of phase control, the ground noise contours for the 2D four propeller layout are given for the different optimization regions in Fig. 9. Clearly, the optimization performs well as it determines phasing combinations to steer the tonal noise away from the ground regions of interest. If phase control is implemented in practice, assuming a noise sensitive area is being passed on the vehicle starboard ($-x_2$), the controller would need to transition consecutively through phase sets given in Figs. 9a,b,c, and finally d during the flyover event. The relative phase values are also given in each figure. While these values are not particularly intuitive, there does seem to be a relationship between Figs. 9a,d and Figs. 9b,c.

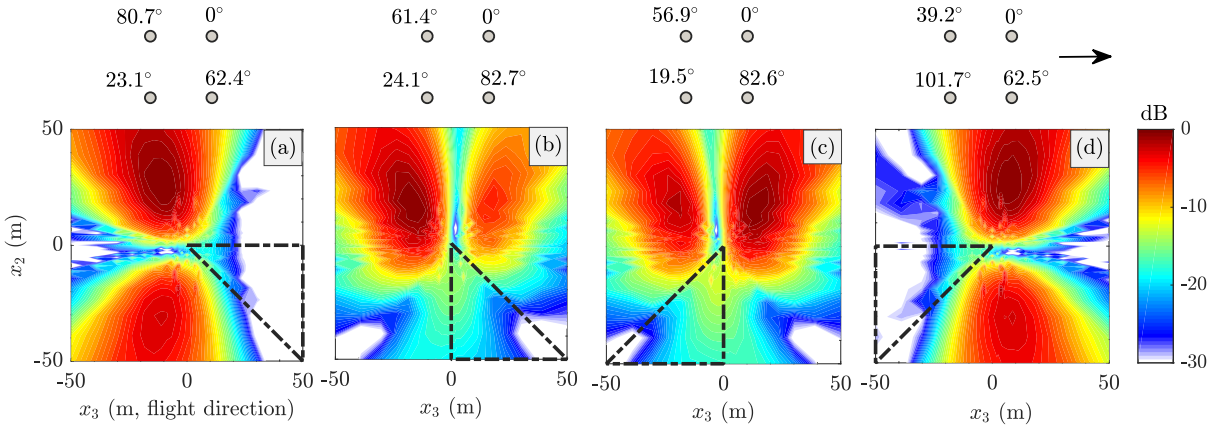

Figure 9. Phase control to minimize noise of the blade passage frequencies in region (a) $\mathcal{Z}_1$, (b) $\mathcal{Z}_2$, (c) $\mathcal{Z}_3$, and (d) $\mathcal{Z}_4$, via relative propeller phase control at 5,000 RPM. The vehicle configuration is the 2D array with $N_p = 4$, and the relative phase, ψ_r, of each propeller is given in degrees. All propellers are rotating clockwise and levels are normalized by the maximum.

The number of propellers is now varied from $N_p = 2$ to 8 for the 2D configuration. The responses to minimize noise in region $\mathcal{Z}_1$ are given in Fig. 10 at 5,000 RPM. When only two propellers are present, the main lobes are wide and thus perform poorly as acoustic energy cannot be fully canceled in the region of interest. However, the effectiveness of four propellers to steer the main lobes away from the ground region of interest is very close to the six or eight propeller cases. For these cases, only a small portion of the lobes remain in the ground region, but with only small differences as the levels approach -20 dB. Thus, if 45° ground wedges are used (as is the case here), there is little additional acoustic benefit to adding propulsors for the 2D configuration.

A similar situation occurs for the 1D configuration as shown in Fig. 11, but with noticeable differences in the ground contours. Again, the benefit flattens as $N_p \geq 4$. Most interesting, in addition to reducing the noise in the region of interest, the optimizer tends to find phasings which steer the majority of the total energy to the opposing side of the vehicle, particularly as N_p is increased. Thus, the 1D array would likely outperform the 2D array if the optimization region is chosen such that it spans the full $-x_2$ plane. This characteristic itself could be leveraged in a powerful way, e.g., in cases when the noise sensitive area remains on one side of the vehicle.

Figure 12 summarizes the parameter space across the two configurations when all propellers are rotating in the same direction. The $\Delta_{\mathcal{Z}_i}$ metric is defined as the average sound pressure level in the specified ground region relative to the reference case defined in section II.E. Note that when the metric is spatially averaged over the ith portion of the ground plane, a subscript $\mathcal{Z}_i$ will be used to delineate from the metric defined in section II.F, which only considers a single point in space. Some obvious trends can be extracted from these plots. Consistent with the previous discussion, the benefit levels off when $N_p \geq 4$ for a given propeller configuration (1D or 2D).

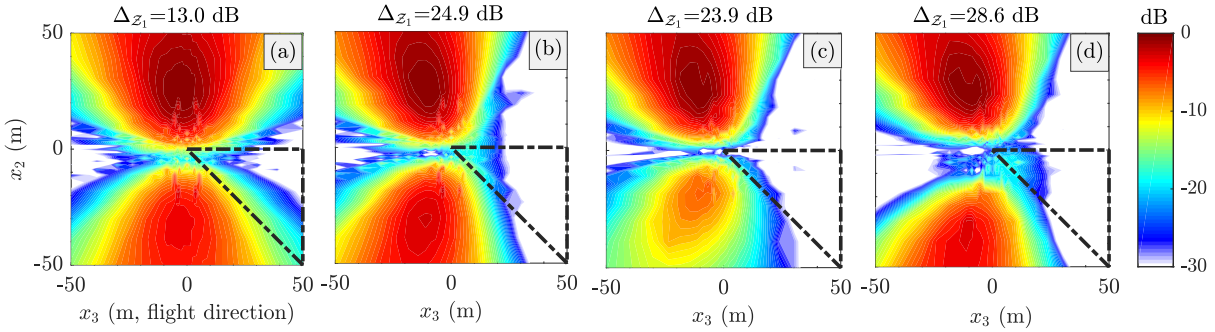

Figure 10. Phase control to minimize noise of the blade passage frequencies in region $\mathcal{Z}_1$, for (a) $N_p = 2$, and the 2D propeller layouts in which (b-c) $N_p = 4$, 6, 8, respectively, at 5,000 RPM. All propellers are rotating clockwise and levels are normalized by the maximum.

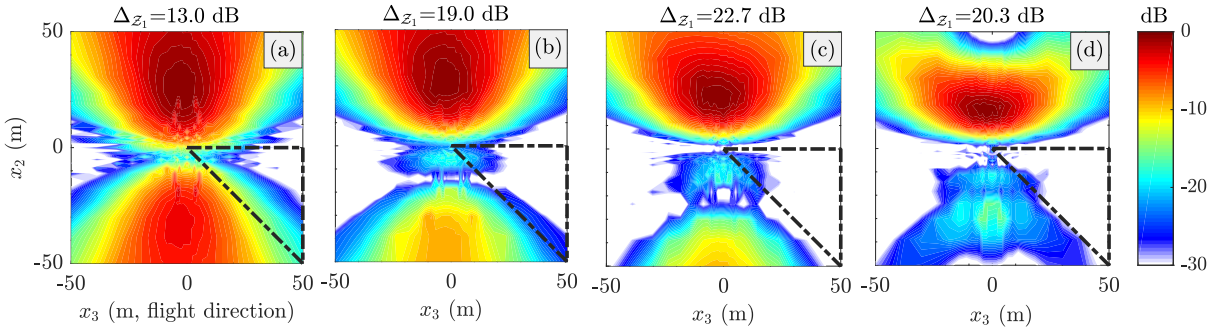

Figure 11. Phase control to minimize noise of the blade passage frequencies in region $\mathcal{Z}_1$, for (a) $N_p = 2$, and the 1D propeller layouts in which (b-c) $N_p = 4$, 6, 8, respectively, at 5,000 RPM. All propellers are rotating clockwise and levels are normalized by the maximum.

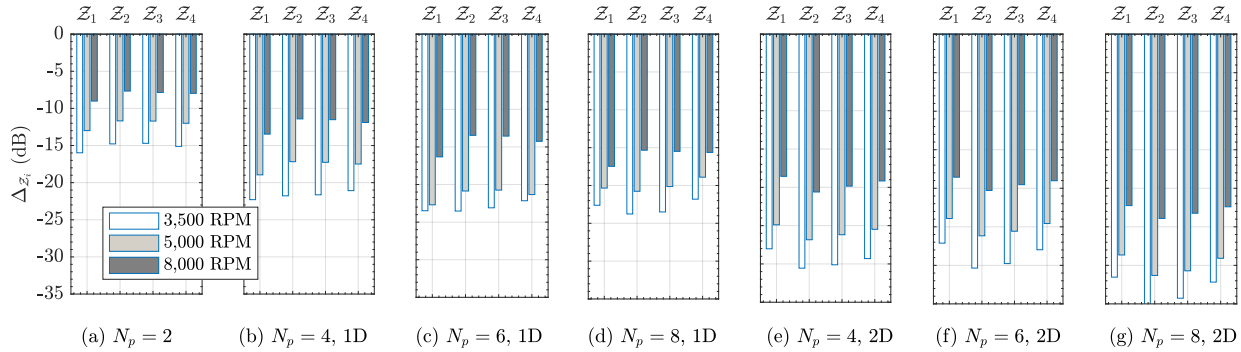

Figure 12. Ideal benefits of phase control to minimize noise of the blade passage frequencies in ground regions $\mathcal{Z}_1$-$\mathcal{Z}_4$, for (a-g) different canonical vehicle configurations, each at three different rotation rates. All propellers are rotating clockwise.

Also, there is a reduction in benefit with an increase in rotation rate for a given configuration (compare $(\Delta)_{\mathcal{Z}_i}$ within one of Figs. 12(a)-(g)). This trend can be attributed to the relationship between the separation distance and the wavelength of the radiating acoustics, quantified by kd – an important parameter to characterize the nominal directivity pattern of combined sources. For the results here, $kd = 1.3 - 3.0$ based

on the blade passage frequency and the distance between adjacent propellers. As kd increases, the lobes in the directivity pattern decrease in angular range and the angle separating adjacent peaks also decreases. Thus, it is more difficult to simultaneously cancel multiple lobes that may cover the ground plane. To show this further, Figure 13 displays the response of the 1D $N_p = 8$ configuration for various RPM (hence, kd) as it best illustrates this dependency. Black contour lines are superposed to assist in visualizing the lobe structures. Another reason for the reduction in benefit with an increase in kd, and perhaps of secondary importance, could be tied to the relative amplitudes of the harmonics relative to the amplitude at f_0. The optimizer used herein only attempts to minimize the rms pressure at f_0 (to limit computational expense) rather than over all tonal components. For a single isolated propeller, the ratio $SPL(f_0) - SPL(2f_0) = 34$ dB at the lowest rotation rate, justifying the optimizer simplification. However, potentially biased benefits could result for the highest rotation rate, as this ratio decreases to 14 dB. Additional analysis would need to be pursued to understand the relative importance of the higher harmonics.

Up to this point, the propellers have been set to rotate in the same direction. However, as captured by the experiments (see Fig. 2), quite different directivity patterns result with counterrotating propellers. Analogous to Fig. 12, Fig. 14 summarizes the parameter space when the $N_p/2$ starboard side propellers are rotating clockwise and the port side are rotating counterclockwise. For a given set of conditions, i.e., comparing Fig. 12b with Fig. 14b, the potential benefits are smaller compared to the case with rotation directions being the same. This is because the distance between the blades of counterrotating propellers are being modulated as they rotate; thus, the relative phase of the radiating acoustics is also being spatially modulated. Ultimately, the degree of coherence of the acoustic waves is reduced in a time-averaged sense. Coarsely speaking, a larger benefit is observed when all propellers are rotating in the same direction, but counterrotating cases are less sensitive to reduction in the potential benefit with increasing kd.

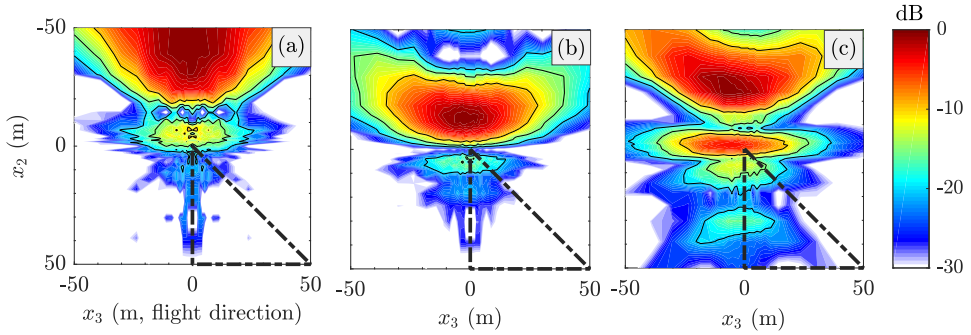

Figure 13. Phase control to minimize the blade passage frequencies in region $\mathcal{Z}_2$, for the 1D configuration, $N_p = 8$, at (a) 3,500, (b) 5,000, (c) 8,000 RPM. All propellers are rotating clockwise and levels are normalized by the maximum; black contour lines are superposed in increments of 5 dB down to -20 dB to highlight differences in lobe patterns.

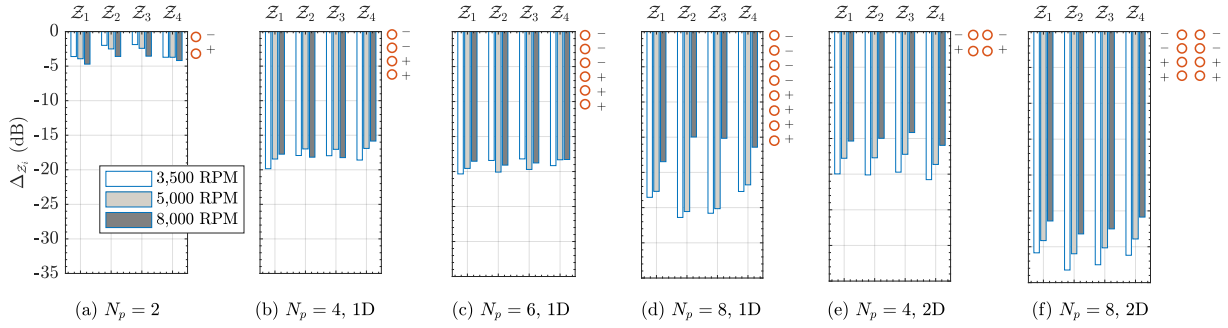

Figure 14. Ideal benefits of phase control to minimize the blade passage frequencies in ground regions $\mathcal{Z}_1$-$\mathcal{Z}_4$, for (a-f) different canonical vehicle configurations, each at three different rotation rates. Rotation directions are both clockwise (+) and counterclockwise (−) as defined in the legends.

III.B. Degradation due to Realistic Effects

The effect of a phase setpoint error is given for different propeller configurations in Fig. 15. The rotation rate is set to 5,000 RPM, and the results are spatially averaged over the optimization ground region $\mathcal{Z}_2$.

While there are differences across the various configurations when the setpoint error is small, all but one configuration ($N_p = 2$, counterrotating) share the same trend. Moreover, the trend is well predicted using equation 6 and can be useful in quickly estimating the allowable error present in the system for a given noise reduction. For example, approximately 6 dB reduction can be achieved if the standard deviation of the Gaussian phase error is 3% ($\sigma(\psi_r)/\psi_{total}$=0.03) relative to the full propeller azimuth. Strictly speaking, this equation should only be used when the pressure amplitudes are equivalent. Amplitudes vary at a given observer due to differences in propagation distances and nonuniform directivity of the individual propellers. However, these differences are small enough to enable a reasonable estimate to be made. Large differences in amplitudes would require the use of equation 8 to provide a better estimate. In any case, it is likely the trends will diverge from these equations if the ground region of interest is made larger or if the rotation rate is increased such that secondary lobe patterns are present (for example, see Fig. 13c).

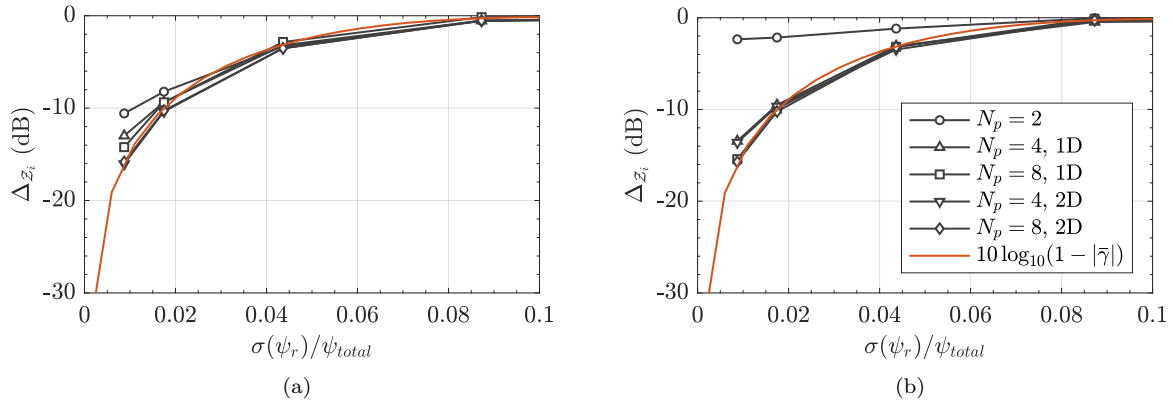

Figure 15. Modeled degradation of potential benefit due to an error in the phase setpoint, given in terms of the standard deviation σ. Example is at 5,000 RPM for region $\mathcal{Z}_2$, for (a) all propellers rotating clockwise and (b) propellers rotating in both clockwise and counterclockwise directions as defined in Fig. 14.

To visually show the effect of the second type of motor control error from equation 10, Fig. 16 gives the ground noise contours optimized for region $\mathcal{Z}_2$ from the two by two propeller array, both with and without error in the motor controller. As expected, increasing the motor control error degrades the noise reduction potential. An error of 0.1% ($\Delta\Omega/\Omega = 0.001$) displays a noticeable but small change relative to the case without error. Acoustic energy begins to leak into the region of interest when increasing the error to 0.3%. For errors greater than 0.8%, nearly all benefit is lost, and the ground contours begin to resemble the reference case.

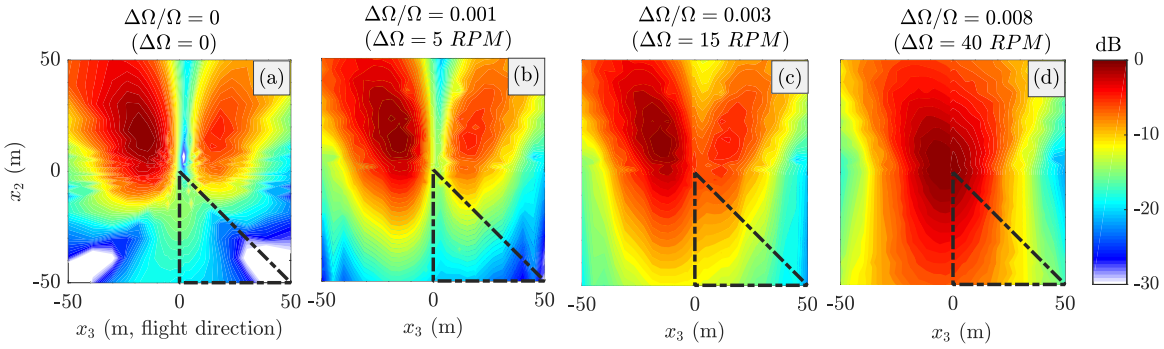

Figure 16. Modeled effect of motor control error on the 2D configuration, $N_p = 4$, 5000 RPM, all rotating clockwise.

Finally, Fig. 17 plots the spatially averaged potential benefit for various propeller configurations as a function of the modulation deviation from the nominal rotation rate. Comparable to the phase setpoint error, the trends here are similar across the configurations as well. Again, equation 6 captures the overall trends. Based on current technology, a 20-30 RPM deviation can be expected (although such an error could potentially be improved). Using the conditions in Fig. 17 and assuming this error, $\Delta\Omega/\Omega \approx 0.005$, yields

$\Delta_{\mathcal{Z}_2} \approx 6$ dB for all propeller configurations. Thus, phase control shows merit as a possible means of noise reduction technology, albeit far from idealized benefits.

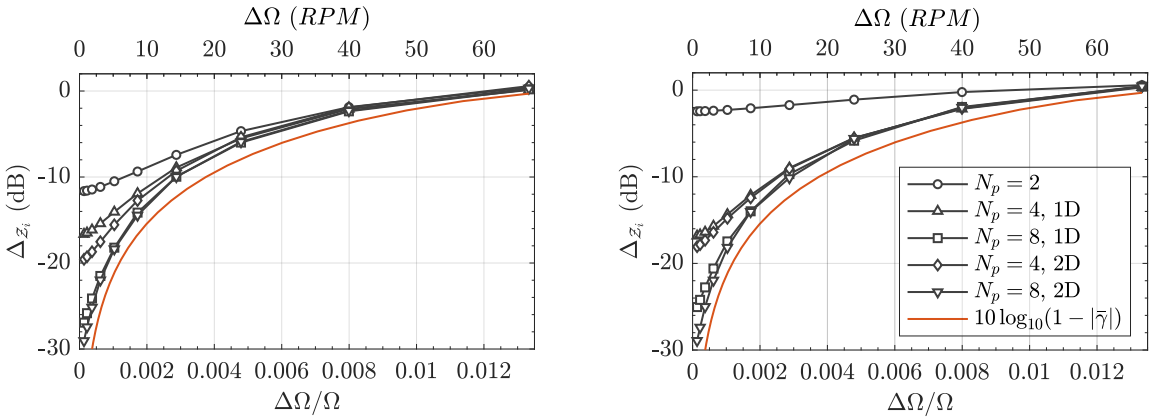

Figure 17. Modeled degradation of potential benefit due to differences in rotation rate. Example is at 5,000 RPM for region $\mathcal{Z}_2$, for (a) all propellers rotating clockwise and (b) propellers rotating in both clockwise and counterclockwise directions as defined in Fig. 14.

Conclusions

A large parameter space was studied to understand limits of performance for a vehicle under phase control. The following list summarizes the observed trends both in an ideal sense, as well as including the sensitivity to error in the motor controller:

- A reasonable reduction is obtained for both 1D and 2D configurations when $N_p \geq 4$; this observation is dependent on the chosen ground plane regions herein. In general, larger N_p will better handle an increase in the angular range of the low-noise region.
- Propeller layouts arranged in the 2D configuration have better overall response to phase control relative to the 1D configuration with respect to the ground plane regions herein. However, if steering the noise away fully from the right or left side of the vehicle is desired, the ground noise contours of the 1D configuration suggest better performance in this situation.
- The potential benefit is reduced with increasing kd; in this paper this value is based on the blade passage frequency and the separation distance between adjacent propellers.
- Coarsely speaking, a larger benefit is observed when all propellers are rotating in the same direction, but counterrotating cases are less sensitive to changes in kd.
- The potential benefits of phase control are sensitive to both an error in a phase setpoint and an error in the rotation rate. To achieve a 6 dB reduction at the blade passage frequency for a three-bladed propeller, the standard deviation of a Gaussian phase error should not exceed approximately 3% of the full azimuth. Similarly, the deviation from the nominal rotation rate should not exceed approximately 0.5%.
- In addition to the geometric observations based on configuration and spacing, rules of thumb can be determined using the generalized magnitude coherence function to understand how "tight" motor control must be to obtain a given noise reduction benefit. The generalized coherence method can estimate the potential benefit as a function of noise in the signal, and will work for systems with more than two propellers (as opposed to the ordinary coherence function which can only handle a pair of signals). Although not studied, equation 8 formulates an extension to include signals of arbitrary amplitudes which would occur, for example, if the propellers are at an angle of attack or if there are differences in collective blade pitch.

Acknowledgments

This work was supported by the NASA Aeronautics Research Mission Directorate, Revolutionary Vertical Lift Technology Project. The authors would like to thank Dr. Nikolas Zawodny for providing the representative propeller acoustic spectra of Fig. 8, and Dr. Jason June for his technical review.

References

[1]Fredericks, W., Moore, M., and Busan, R., "Benefits of Hybrid-Electric Propulsion to Achieve 4X Increase in Cruise Efficiency for a VTOL Aircraft," *AIAA Aviation Technology, Integration, and Operations (ATIO) Conference*, AIAA Paper 2013-4324, 2013.

[2]"Airbus Ventures, Vahana," https://www.airbus-sv.com/projects/1, Accessed: November 1, 2018.

[3]"Joby Aviation," www.jobyaviation.com/, Accessed: November 1, 2018.

[4]Zawodny, N., Boyd, D., and Burley, C., "Acoustic Characterization and Prediction of Representative, Small-Scale Rotary-Wing Unmanned Aircraft System Components," *72nd American Helicopter Society (AHS) Annual Forum*, 2016.

[5]Intaratep, N., Alexander, W., Devenport, W., Grace, S., and Dropkin, A., "Experimental study of quadcopter acoustics and performance at static thrust conditions," *22nd AIAA/CEAS Aeroacoustics Conference*, AIAA Paper 2016-2873, 2016.

[6]Tinney, C. E. and Sirohi, J., "Multirotor Drone Noise at Static Thrust," *AIAA Journal*, 2018, pp. 1–11.

[7]Huff, D., Henderson, B., and Envia, E., "Motor Noise for Electric Powered Aircraft," *22nd AIAA/CEAS Aeroacoustics Conference*, AIAA Paper 2016-2882, 2016.

[8]Zawodny, N. and Boyd, D., "Investigation of Rotor-Airframe Interaction Noise Associated with Small-Scale Rotary-Wing Unmanned Aircraft Systems," *73rd AHS Annual Forum and Technology Display*, 2017.

[9]Pascioni, K. and Rizzi, S., "Tonal Noise Prediction of an Unmanned Aerial Vehicle," *24th AIAA/CEAS Aeroacoustics Conference (39th AIAA Aeroacoustics Conference)*, AIAA Paper 2018-2951, 2018.

[10]Pascioni, K., Rizzi, S., and Aumann, A., "Auralization of an Unmanned Aerial Vehicle under Phase Control," *47th International Congress and Exposition on Noise Control Engineering*, 2018.

[11]Johnston, J., Donham, R., and Guinn, W., "Propeller signatures and their use," *Journal of Aircraft*, Vol. 18, 1981, pp. 934–942.

[12]Magliozzi, B., "Synchrophasing for Cabin Noise Reduction of Propeller-Driven Airplanes," *8th AIAA Aeroacoustics Conference*, AIAA Paper 1983-0717, 1983.

[13]Nguygen, C. and Kelly, J., "A Users Guide for the NASA ANOPP Propeller Analysis System," NASA CR-4768, 1997.

[14]Zorumski, W., "Aircraft Noise Prediction Program Theoretical Manual, Part 1," NASA TM-93199, 1982.

[15]Farassat, F., "Theory of Noise Generation from Moving Bodies with an Application to Helicopter Rotors," NASA TR-R-451, 1975.

[16]Grosveld, F., "Calibration of the structural acoustics loads and transmission facility at NASA Langley Research Center," *INTER-NOISE and NOISE-CON Congress and Conference Proceedings*, Vol. 1999, Institute of Noise Control Engineering, 1999, pp. 1541–1546.

[17]Schiller, N., Pascioni, K., and Zawodny, N., "Tonal Noise Control using Phased Rotors," *Vertical Flight Society 75th Annual Forum & Technology Display*, in progress, 2019.

[18]Blackstock, D., *Fundamentals of Physical Acoustics*, John Wiley & Sons, 2000.

[19]Ares-Pena, F., Rodriguez-Gonzalez, J., Villanueva-Lopez, E., and Rengarajan, S., "Genetic algorithms in the design and optimization of antenna array patterns," *IEEE Transactions on Antennas and Propagation*, Vol. 47, No. 3, 1999, pp. 506–510.

[20]Boeringer, D. and Werner, D., "Particle swarm optimization versus genetic algorithms for phased array synthesis," *IEEE Transactions on antennas and propagation*, Vol. 52, No. 3, 2004, pp. 771–779.

[21]Byrd, R., Gilbert, J., and Nocedal, J., "A trust region method based on interior point techniques for nonlinear programming," *Mathematical Programming*, Vol. 89, No. 1, 2000, pp. 149–185.

[22]The Mathworks, Inc., Natick, Massachusetts, *MATLAB Optimization Toolbox, version 9.3.0.713579 (R2017b)*, 2017.

[23]Sobol, I., "On the distribution of points in a cube and the approximate evaluation of integrals," *Zhurnal Vychislitel'noi Matematiki i Matematicheskoi Fiziki*, Vol. 7, No. 4, 1967, pp. 784–802.

[24]Saha, S., *Aperture synthesis: methods and applications to optical astronomy*, Springer Science & Business Media, 2010.

[25]Ramirez, D., Via, J., and Santamaria, I., "A generalization of the magnitude squared coherence spectrum for more than two signals: definition, properties and estimation," *IEEE International Conference on Acoustics, Speech and Signal Processing*, IEEE, 2008, pp. 3769–3772.

[26]Rizzi, S., Palumbo, D., Rathsam, J., Christian, A., and Rafaelof, M., "Annoyance to Noise Produced by a Distributed Electric Propulsion High-Lift System," *23rd AIAA/CEAS Aeroacoustics Conference*, AIAA Paper 2017-4050, 2017.

[27]Zawodny, N. and Haskin, H., "Small Propeller and Rotor Testing Capabilities of the NASA Langley Low Speed Aeroacoustic Wind Tunnel," *23rd AIAA/CEAS Aeroacoustics Conference*, AIAA Paper 2017-3709, 2017.